Double-folding interaction for ^{6}He + α scattering

D. Baye, L. Desorgher,* D. Guillain, and D. Herschkowitz
Physique Nucléaire Théorique et Physique Mathématique, Code Postal 229, Université Libre de Bruxelles, B 1050 Brussels, Belgium
(Received 2 May 1996)

In order to prepare the analysis of planned elastic-scattering experiments with a low-energy radioactive ^{6}He beam on an α target, we determine a theoretical interaction between these nuclei. A double-folding potential is obtained from a realistic ^{6}He density derived from a microscopic three-cluster model. Special attention is paid to the ^{6}He-halo description. The resulting potential displays an unusual long tail which might have observable effects on the elastic cross sections. The parity dependence of the optical potential related to the elastic transfer of the halo neutrons is discussed qualitatively. [S0556-2813(96)05811-6]

PACS number(s): 25.60.Bx, 21.60.Gx, 24.10.Ht, 25.55.Ci

I. INTRODUCTION

With the advent of low-energy radioactive nuclear beams, new collisions are, or will soon become, available for elastic-scattering studies [1]. They provide new types of confrontations between theory and experiment, which allow the exploration of the isospin degree of freedom in collisions. Of particular interest is the development of low-energy ^{6}He beams which offers a new way of exploring halo properties. Indeed, ^{6}He is the simplest nucleus exhibiting an anomalously large matter radius [2]. This property is indicative of the existence of a neutron halo [3], i.e., of a region of space where loosely bound neutrons have a significant probability of presence at a large distance from the other nucleons. Until now the halo properties have been mostly explored in high-energy collisions [4,5] with, however, the noticeable exception of delayed β-decay modes [6]. Low-energy elastic scattering should reveal new aspects of the ^{6}He two-neutron halo. The long tail of the nuclear density should have observable consequences on the cross sections, even in the vicinity of the Coulomb barrier.

Among several possible candidates, the ^{6}He + α collision which is being planned at Louvain-la-Neuve is particularly interesting. Two possible striking physical effects will deserve attention: an unusually long range of the nucleus-nucleus potential and a rather strong parity effect corresponding to the elastic transfer [7,1] of the halo neutrons. Both effects are a direct consequence of the halo existence and should provide a new insight into its properties. However, the low intensity of the available ^{6}He beam, when compared with stable-beam intensities, will lead to relatively large error bars on the measured cross sections because of a lack of statistics. The first measurements will most likely not allow accurate phase-shift analyses in spite of the low number of contributing partial waves. They may even not allow an unambiguous optical-model fit. However, they will be invaluable for the validation or invalidation of model calculations of the ^{6}He wave function and of the ^{6}He + α scattering.

The aim of the present work is to prepare the search for a ^{6}He + α interaction by calculating a double-folding approximation of its real part. In this model, ^{6}He is described in a realistic way but antisymmetrization effects between the colliding nuclei are neglected. The resulting real potential should provide a good starting point for a fit of a phenomenological potential to the expected data. In addition, the tail of the double-folding potential will provide a test of future fully microscopic calculations of ^{6}He + α scattering. Indeed, the microscopic cluster model [8,9] is very efficient in explaining the scattering of light ions. Its application to ^{6}He + α scattering should lead to a quite realistic evaluation of its phase shifts and cross sections. However, such calculations face several difficulties, because of the complicated microscopic treatment of the ^{6}He wave function [10–12] and of the low binding energy of ^{6}He (0.975 MeV) which may render single-channel approaches insufficient. The effects of the antisymmetrization between the ^{6}He and α nuclei become negligible at large distances and the effective potentials of a fully microscopic model tend towards a double-folding interaction [13].

The main ingredient we need is an accurate density for ^{6}He. Although accurate nonmicroscopic models exist [14,15], we choose to calculate it in a microscopic three-cluster model for which a minimal number of assumptions is required. This model which was first applied to ^{6}He [16] also provided useful information on the ^{14}Be [17], ^{17}B [18], and ^{17}Ne [19] halo nuclei or candidate halo nuclei. It is based on a large linear combination of three-cluster basis states projected on the total angular momentum and on parity. The microscopic ^{6}He wave function of Ref. [16] proved useful in analyzing the delayed β decay of ^{6}He [20] and dissociation cross sections of this nucleus [21] but better approximations based on different variants of the microscopic cluster model are now available [10–12] (an attempt to get rid of the cluster assumption can be found in Ref. [22]). In the present work, the ^{6}He wave function of Ref. [16] is improved and used to calculate a realistic ^{6}He density.

Section II is devoted to a summary of the three-cluster model and a description of the basis choice. The obtained energy and radius are discussed. The corresponding density is calculated in Sec. III. In Sec. IV, a double-folding ^{6}He + α interaction is determined and the importance of the parity

*Present address: Paul Scherrer Institute, CH-5232 Villigen, Switzerland.

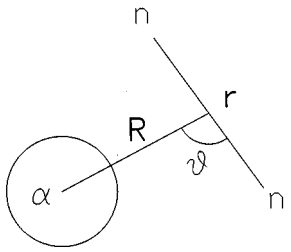

FIG. 1. Schematic definition of the generator coordinates **r**, **R**, and θ.

component of the optical potential is estimated. Concluding remarks are presented in Sec. V.

II. MICROSCOPIC THREE-CLUSTER ^{6}He WAVE FUNCTION

The ^{6}He nucleus is assumed to be described by three clusters, i.e., an α cluster made of two protons and two neutrons in $0s$ harmonic-oscillator orbitals, and two single-neutron clusters. Basis states differ by the relative locations of these clusters. After proper projection of such basis states on good quantum numbers, this basis is employed in a variational calculation with the microscopic Hamiltonian

$$H=\sum_{i=1}^{6} T_i+\sum_{i>j=1}^{6} V_{ij}. \tag{1}$$

In this expression, T_i is the kinetic energy of nucleon i with coordinate $\mathbf{r}_i$, and V_{ij} is an effective nucleon-nucleon interaction which involves central and spin-orbit terms. The Coulomb interaction is neglected as it only affects the internal energy of the α cluster and not the relative motions of the three clusters.

The intrinsic three-cluster basis functions are defined as

$$\Phi_{SM_S}(\mathbf{r},\mathbf{R})=\mathcal{A}\Phi_\alpha(-\tfrac{1}{3}\mathbf{R})[\Phi_n(\tfrac{2}{3}\mathbf{R}+\tfrac{1}{2}\mathbf{r})\otimes\Phi_n(\tfrac{2}{3}\mathbf{R}-\tfrac{1}{2}\mathbf{r})]^{SM_S}, \tag{2}$$

where $\mathcal{A}$ is the antisymmetrization projector over the six nucleons. The Slater determinant $\Phi_\alpha(\mathbf{X})$ involves four $0s$ harmonic-oscillator orbitals centered at $\mathbf{X}$. Each function $\Phi_n(\mathbf{X})$ represents a neutron in a $0s$ oscillator orbital centered at $\mathbf{X}$ with spin 1/2. They share the same oscillator parameter b with Φ_α. The generator coordinate $\mathbf{r}$ is a geometrical parameter which defines the relative locations of the neutron clusters while the generator coordinate $\mathbf{R}$ defines the location of the center of mass (c.m.) of the neutron clusters with respect to the center of the α cluster (see Fig. 1). In Eq. (2), the neutron spins are coupled to the total spin S with projection M_S.

The nonorthogonal basis functions of the model are obtained by projecting the intrinsic functions (2) on the total angular momentum $J=0$ and on positive parity. We choose the z axis along the line joining the α center and a neutron center, and the x axis in the plane of the three centers. In this model space, the action of the parity operator Π on an intrinsic state is equivalent to a rotation by an angle of π around the y axis,

$$\Pi\Phi_{SM_S}(\mathbf{r},\mathbf{R})=\exp(-i\pi L_y)\Phi_{SM_S}(\mathbf{r},\mathbf{R})=\Phi_{SM_S}(-\mathbf{r},-\mathbf{R}). \tag{3}$$

Denoting by $P_K^{LM\pi}$ the projector on parity π and on the total *orbital* momentum L, one obtains

$$(P_K^{LM\pi}\Phi_{SM_S})(r,R,\theta)=\frac{1}{2}\int[D^{L\star}_{KM}(\Omega)+\pi(-1)^{L-K}D^{L\star}_{-KM}(\Omega)]\times\Phi_{SM_S}(\mathbf{r}_\Omega,\mathbf{R}_\Omega)d\Omega, \tag{4}$$

where Ω represents the three Euler angles α, β, and γ, and θ is the angle between $\mathbf{r}$ and $\mathbf{R}$. The notations $\boldsymbol{r}_\Omega$ and $\boldsymbol{R}_\Omega$ correspond to generator coordinates undergoing a rotation Ω. Because of parity projection, not all values of the body-fixed projection K are useful. For $L=0$, only $K=0$ and $\pi=+$ are possible. For $L=1$ and $\pi=+$, components with $K=0$ vanish while components with $K=+1$ and $K=-1$ are identical. The number K can therefore be omitted and, after coupling L and S, one obtains two types of 0^+ basis states,

$$\Phi_0^{0^+}(r,R,\theta)=\int\Phi_{00}(\mathbf{r}_\Omega,\mathbf{R}_\Omega)d\Omega \tag{5}$$

and

$$\Phi_1^{0^+}(r,R,\theta)=(2\sqrt{3})^{-1}\sum_{M_S}(-1)^{M_S+1}\times\int[D^{1\star}_{1-M_S}(\Omega)+D^{1\star}_{-1-M_S}(\Omega)]\times\Phi_{1M_S}(\mathbf{r}_\Omega,\mathbf{R}_\Omega)d\Omega, \tag{6}$$

according to the value S of the total intrinsic spin. In the following, we shall collectively denote the generator coordinates $(\mathbf{r},\mathbf{R})$ by $\boldsymbol{\lambda}$ and (r,R,θ) by λ.

The general trial wave function is written as

$$\Psi^{0^+}=\Psi_0^{0^+}+\Psi_1^{0^+}, \tag{7}$$

with

$$\Psi_S^{0^+}=\sum_n C_n^S\Phi_S^{0^+}(\lambda_n), \tag{8}$$

where the sum runs over different selected sets $\lambda_n\equiv(r_i,R_j,\theta_k)$ of generator coordinates. The variational coefficients are determined by solving the system of linear equations

$$\sum_S\sum_n\langle\Phi_{S'}^{0^+}(\lambda_{n'})|H-E|\Phi_S^{0^+}(\lambda_n)\rangle C_n^S=0. \tag{9}$$

The matrix elements appearing in Eq. (9) can be obtained with standard projection techniques [23]. They involve a triple integration over the Euler angles. For an operator O

which does not couple different spin values, the Wigner-Eckart theorem in spin space and the definitions (5) and (6) provide

$$\langle \Phi^{0^+}_{S'}(\lambda')|O|\Phi^{0^+}_{S}(\lambda)\rangle = \delta_{SS'}\int f_S(\Omega)\langle \Phi_{SM_S}(\boldsymbol{\lambda}')|O|\Phi_{SM_S}(\boldsymbol{\lambda}_\Omega)\rangle d\Omega, \tag{10}$$

with M_S arbitrary, and

$$f_0 = \tfrac{1}{2}, \tag{11}$$

$$f_1 = \tfrac{1}{2}\sum_{M,M'=\pm 1} D^{1\star}_{MM'}(\Omega) = \cos\alpha\cos\gamma - \sin\alpha\sin\gamma\cos\beta. \tag{12}$$

The intrinsic matrix element in Eq. (10) is calculated analytically (or could be calculated numerically) with Slater-determinant techniques [23]. For the spin-orbit term of the nuclear force, an expression similar to Eq. (10) but involving several matrix elements, between different spin states, is also established.

The angular integration in Eq. (10) is performed numerically with a triple Gauss quadrature [24]. For the α and γ angles, the Gauss-Fourier method, i.e., equally spaced mesh points [25], is employed with 12–24 points. For β, the Gauss-Legendre quadrature with 24 points is used. The total number of integration points can be reduced by a factor of 2 because the cluster centers belong to a same plane.

In an early microscopic calculation of ^{6}He with the present model [16,20], the number of sets λ_n was restricted and their selection was rather empirical. The fact that the halo was not well enough described at large distances appeared in a study of the β-delayed deuteron decay of ^{6}He [20]. This process is sensitive to the halo behavior up to distances larger than 10 fm. Other observables such as dissociation cross sections were described in a satisfactory way [21]. In the present work, we adopt the stochastic selection of generator coordinates proposed in Ref. [26] and first applied to microscopic descriptions of halo nuclei in Ref. [11]. Notice that the definitions of generator coordinates are different in both models. In Ref. [11], the stochastic approach is applied to widths of Gaussian basis functions describing the relative motions of the halo neutrons and of the α cluster. A similar procedure has been adopted in the present case. Triplets λ_n of generator coordinates are selected randomly (with some weight functions for r_i and R_j) and tested in the basis. When they satisfy an energy-improvement criterion, they are kept in the basis. Otherwise, a new triplet is tested. At some stages, we have reconsidered the marginal utility of each basis state in order to remove redundancies. It occurred that accepted triplets had, after a significant enlargement of the basis, a weak influence on the final results. Such triplets were dropped.

The calculation is performed with the Minnesota interaction [27,13] including a spin-orbit term. The central part of this interaction reads

$$V = [V_R + \tfrac{1}{2}(1+P_\sigma)V_t + \tfrac{1}{2}(1-P_\sigma)V_s] \times [\tfrac{1}{2}u - \tfrac{1}{2}(2-u)P_\sigma P_\tau], \tag{13}$$

where V_R, V_t, and V_s are the repulsive-core, triplet, and singlet Gaussian form factors, respectively. The exchange parameter u is kept free while the zero-range spin-orbit strength $S_0 = 40$ MeV fm^5 [28] (J_λ in the notations of Ref. [13]) is fixed with the $\alpha+n$ system. The harmonic-oscillator parameter $b = 1.28$ fm is selected, which corresponds to the minimum energy -25.58 MeV of the α cluster with the Minnesota interaction. A basis of 65 functions is constructed with the stochastic technique described above. In order to save computer time, the basis-state selection was applied with the central part of the interaction only. The spin-orbit term was added when the basis was obtained.

Comparing microscopic calculations of the literature with the present one is rather difficult because the model assumptions are usually different. In particular, comparing radii when the binding energies are not close to each other is meaningless since the tail of the wave function contributes to the radius. In Ref. [10], the calculation involves spin-orbit and tensor interactions, a distortion of the α cluster, and a ^{3}H + ^{3}H configuration. That work shows that the ^{3}H + ^{3}H channel introduces a significant improvement but the $\alpha+n+n$ variational basis for the halo description is more restricted than in other microscopic calculations. A comparison with the present work is made impossible by the α cluster distortion which requires rather different conditions for the force. The model of Refs. [11] and [12] is much closer to the present one, except for the lack of spin-orbit interaction. The main difference between both models lies in the basis choice which allows more freedom for the configuration choices in the quoted references with an additional internal angular momentum between the α cluster and a neutron (Y states) or between the neutrons (T states), but a much simpler technique of calculation in the present work. Therefore we first switch the spin-orbit interaction off and choose $u = 1.14$ as in Ref. [11] (the oscillator parameter and the central force are then identical). The stochastic technique for the choice of parameters is also similar. The binding energy we obtain (0.53 MeV) is significantly less good than the best result of that work (1.02 MeV). Convergence is much slower with the present basis. It is comparable to, but slightly better than, the result obtained with the T basis functions of Varga *et al.* (0.40 MeV). The members of the other family of basis functions in Ref. [11] (Y functions) are very efficient to speed up convergence. Such functions have no equivalent in the present model.

We now turn to the calculation with the spin-orbit interaction. We obtain the reasonable value $u = 0.96$ in order to reproduce the experimental binding energy (0.98 MeV). An $S = 1$ component contributes by about 2.53 MeV. This means that the binding would not be ensured without spin-orbit force. The corresponding matter radius is 2.23 fm. The $S = 1$ probability is 17.4%, i.e., close to the value 16% obtained in the three-particle nonmicroscopic model of Ref. [15] with an effective $\alpha+n$ interaction and with the same Minnesota interaction between the halo neutrons.

III. MATTER DENSITY OF ^{6}He

In order to calculate a double-folding interaction, one needs a matter density for ^{6}He. This density at location **r** is given by

$$\rho(r)=\left\langle \Psi^{0^+}\left|\sum_{j=1}^{6}\delta(\mathbf{r}_j-\mathbf{R}_{\text{c.m.}}-\mathbf{r})\right|\Psi^{0^+}\right\rangle, \tag{14}$$

where $\mathbf{R}_{\text{c.m.}}=\frac{1}{6}\Sigma_j \mathrm{r}_j$ is the c.m. coordinate of the six nucleons. Rotation invariance entails that ρ only depends on the norm of $\mathbf{r}$. The standard normalization

$$4\pi\int_0^\infty \rho(r)r^2dr=6 \tag{15}$$

to the mass number is applied.

In principle, Eq. (14) is valid for wave functions which do not depend on $\mathbf{R}_{\text{c.m.}}$. However, the intrinsic basis functions (2) present the factorization property

$$\Phi_{SM_S}(\mathbf{r},\mathbf{R})=\phi_{\text{c.m.}}\phi_{\text{int}}(\mathbf{r},\mathbf{R}), \tag{16}$$

where $\phi_{\text{c.m.}}$ is a Gaussian function depending only on the c.m. coordinate $\mathbf{R}_{\text{c.m.}}$. The fact that $\phi_{\text{c.m.}}$ does not depend on the generator coordinates results from the way they are defined in Eq. (2). Because of this factorization property, the density formula (14) is also valid for the present wave functions in spite of their spurious c.m. dependence. There remains, however, a drawback: The operator in Eq. (14) is not a one-body operator. Therefore, a direct calculation of the density is not convenient. The matrix element (14) can be calculated in momentum space with the following procedure. The Fourier transform of the matrix element of the one-body operator $\Sigma_j\delta(\mathbf{r}_j-\mathbf{r})$ is factorizable into a simple c.m. factor and the Fourier transform of $\rho(r)$. This oscillator-strength matrix element is easily calculated and the spurious c.m. component is simply eliminated with a division. The density is then obtained with an inverse Fourier transform. As already observed in Ref. [29], the final expression for $\rho(r)$ can be formally expressed as a function of an effective one-body operator as

$$\rho(r)=\left\langle \Psi^{0^+}\left|\sum_{j=1}^{6}O_{\text{eff}}(\mathbf{r}_j,r)\right|\Psi^{0^+}\right\rangle. \tag{17}$$

The matrix element (17) can be calculated with the standard cofactor technique [23] with effective one-body matrix elements. Let $\varphi(\mathbf{r}_j,\mathbf{X})$ be a $0s$ harmonic oscillator orbital centered at $\mathbf{X}$ such as those appearing in the basis functions (2). The effective one-body matrix elements are given as in Ref. [29] by

$$\begin{aligned}&\langle\varphi(\mathbf{r}_j,\mathbf{X}')|O_{\text{eff}}(\mathbf{r}_j,r)|\varphi(\mathrm{r}_j,\mathbf{X})\rangle\\&\quad=(2/\pi B^3)\exp[-(\mathbf{X}'-\mathbf{X})^2/4b^2]\\&\qquad\times\exp\{-[4r^2+(\mathbf{X}'+\mathbf{X})^2]/4B^2\}i_0(r|\mathbf{X}'+\mathbf{X}|/B^2),\end{aligned} \tag{18}$$

where $i_0(x)=\sinh x/x$ and $B^2=5b^2/6$. The factor 5/6 results from the c.m. elimination.

Since the density operator does not depend on spin, the two-spin components of Ψ^{0^+} contribute separately and ρ can be split as

$$\rho(r)=\rho_0(r)+\rho_1(r). \tag{19}$$

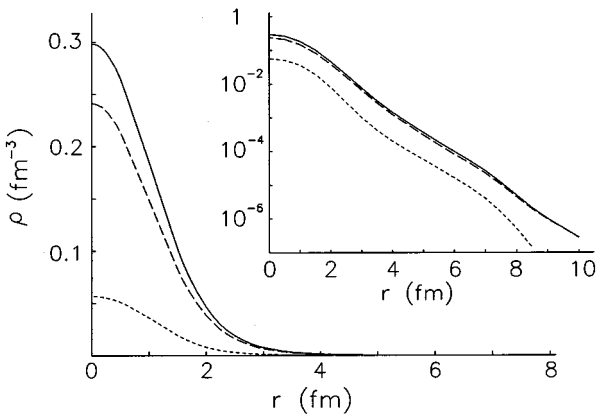

FIG. 2. Microscopic ^{6}He densities ρ (solid lines), ρ_0 (dashed lines), and ρ_1 (dotted lines), in linear and logarithmic scales.

Using Eqs. (8), (10), and (17), the spin-S density reads

$$\begin{aligned}\rho_S(r)=&\sum_{n'}\sum_{n}C^S_{n'}C^S_n\int f_S(\Omega)\\&\times\left\langle\Phi_{SM_S}(\boldsymbol{\lambda}_{n'})\left|\sum_{j=1}^{6}O_{\text{eff}}(\mathbf{r}_j,r)\right|\Phi_{SM_S}(\boldsymbol{\lambda}_{n\Omega})\right\rangle d\Omega.\end{aligned} \tag{20}$$

These partial densities allow one to calculate different observables mentioned in Sec. II such as the rms radius. For example, the spin-1 probability

$$P(S=1)=\frac{2\pi}{3}\int_0^\infty\rho_1(r)r^2dr \tag{21}$$

can be obtained from Eq. (20). We have checked that these densities provide the same rms radius and $S=1$ probability as in Sec. II.

The integrands in expressions (20) are calculated analytically with the cofactor technique and Eq. (18). The triple integration is performed numerically as in Sec. II. The obtained densities ρ (solid lines), ρ_0 (dashed lines), and ρ_1 (dotted lines) are displayed in Fig. 2. Their properties are better seen with a logarithmic scale. The density ρ_1 appears to be essentially proportional to ρ_0 up to $r=8$ fm with a proportionality factor of about one-fifth, i.e., in agreement with $P(S=1)$. At larger distances, ρ_0 and ρ_1 behave differently. In spite of the use of a Gaussian basis, the density presents an almost exponential decrease up to values larger than 10 fm. This confirms that the halo is well covered by the basis functions. We expect the exponential decrease to transform into a Gaussian decrease at distances larger than the largest value of the generator coordinate R. This is indeed the behavior of the calculated density beyond 14 fm. A weak modulation of the decrease can be observed in Fig. 2 beyond 7 fm. It may indicate irregularities in the way the stochastic approach has paved the basis space at large distances. If the average asymptotic decrease is fitted with an exponential $\exp(-r/a)$, one obtains $a=0.7$ fm.

IV. DOUBLE-FOLDING INTERACTION

With the help of the microscopic ^{6}He density, we can now determine a double-folding interaction between two nuclei at a distance R with

$$V_{\rm DF}(R)=\int d\mathbf{r}\rho(r)\int d\mathbf{r}'\rho_\alpha(r')V_{NN}(\mathbf{r}-\mathbf{r}'+\mathbf{R}). \quad (22)$$

In order to remain consistent, we employ the same Minnesota nucleon-nucleon interaction as used for the calculation of the density. In Eq. (22), the quantity denoted as V_{NN} results from an average over the spin and isospin degrees of freedom, of the interaction defined in Eq. (13). Because of the closed shell of the α particle, the result of the spin-isospin part of the calculation is simple and can be summarized as

$$P_\sigma\rightarrow\tfrac{1}{2},\quad P_\tau\rightarrow\tfrac{1}{2}. \quad (23)$$

Hence, the interaction V_{NN} in Eq. (22) reads

$$V_{NN}(r)=\tfrac{1}{16}[(10u-4)V_R+(9u-6)V_t+(u+2)V_s], \quad (24)$$

where V_R, V_t, and V_s are defined as in Eq. (13) [27].

For the α density ρ_α, we choose the density of the α cluster which constitutes the ^{6}He core, i.e.,

$$\rho_\alpha(r)=4(3\pi b^2/4)^{-3/2}\exp(-4r^2/3b^2), \quad (25)$$

with $b=1.28$ fm as before. The integral over $\mathbf{r}'$ in Eq. (22) is then easily performed analytically, as well as the integral over the angular part of $\mathbf{r}$. The final expression is a one-dimensional integral. For a Gaussian term $\exp(-r^2/\nu^2)$ of V_{NN}, the corresponding term $v_{\rm DF}$ of $V_{\rm DF}$ reads

$$v_{\rm DF}(R)=4\pi\int_0^\infty\rho(r)v_{\alpha 0}(r,R)r^2dr, \quad (26)$$

where

$$v_{\alpha 0}(r,R)=4\left(\frac{\nu^2}{\frac{3}{4}b^2+\nu^2}\right)^{3/2}\times\exp\left(-\frac{r^2+R^2}{\frac{3}{4}b^2+\nu^2}\right)i_0\left(\frac{2rR}{\frac{3}{4}b^2+\nu^2}\right). \quad (27)$$

The double-folding potential is then obtained with a numerical quadrature.

The resulting potential is displayed in Fig. 3 (solid lines), where it is compared with the $\alpha+\alpha$ potential of Ref. [30] (dashed lines) and a double-folding $\alpha+\alpha$ potential (dotted lines) obtained from Eqs. (26) and (25). The $\alpha+\alpha$ potentials have similar shapes but different depths. The double-folding model with the Minnesota interaction predicts the phenomenological potential up to some readjustment of its depth which could be estimated by fitting the ^{8}Be ground-state energy. The depth and shape of $V_{\rm DF}$ for ^{6}He + α are generally consistent with the $\alpha+\alpha$ case. However, because of the halo, the influence of the potential extends over a much larger distance. The potential can be well approximated by a Woods-Saxon potential fitting its long-range part plus a Gaussian potential for its short-range part,

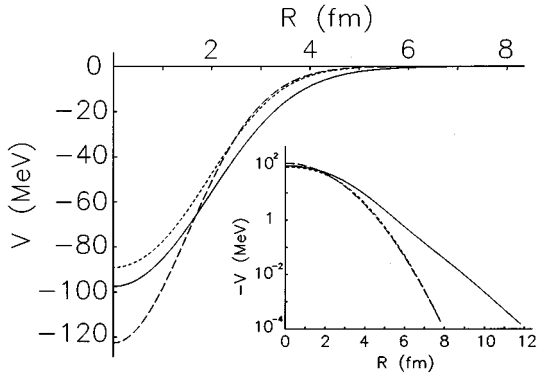

FIG. 3. Double-folding ^{6}He + α potential (solid lines) compared with the corresponding double-folding α + α potential (dotted lines), and with the realistic α + α potential of Ref. [30] (dashed lines).

$$V_{\rm DF}(R)=-V_G\exp(-R^2/a_G^2)-V_S\{1+\exp[(R-R_S)/a_S]\}^{-1}, \quad (28)$$

with $V_G=41.20$ MeV, $a_G=1.95$ fm, $V_S=58.52$ MeV, $a_S=0.725$ fm, and $R_S=2.647$ fm. The difference between the numerical potential and its analytical approximation is everywhere smaller than about 0.6 MeV, this upper value being only reached or approached near the origin.

In this potential the long-range part should not be affected by antisymmetrization effects except for the parity term discussed below. Therefore, we suggest to use it with V_G as a single free parameter in order to correct for antisymmetrization effects. The importance of this correction can be estimated by looking at the spectroscopic properties of this potential. As discussed, e.g., in Ref. [30], such a deep potential provides a number of nonphysical solutions which simulate forbidden states of the ^{6}He + α system, i.e., states of the relative motion which are not allowed by the Pauli principle [8,9]. The number of such states can be evaluated analytically and is here equal to 2 for $l=0$ and 1, and one for $l=2$ and 3. Although the potential is not dedicated to a spectroscopic study of ^{10}Be, it offers a fair qualitative description of its spectrum. The Coulomb interaction defined in Ref. [30] for the α + α system is added to the nuclear potential. In order to reproduce the ^{10}Be ground-state energy, the parameter of the Gaussian part in $V_{\rm DF}(R)$ is modified into the value $V_G=46.6$ MeV. The depth of the potential (28) is increased by about 5%. For $l=0$, the deep potential contains three bound states. The lowest two states at -67.3 and -32.8 MeV simulate the $l=0$ forbidden states of the ^{6}He + α system. The third state (which is fitted) is interpreted as an approximation of the ^{10}Be ground state at -7.43 MeV with

respect to the ^{6}He + α threshold. In the same way, after eliminating the forbidden states in the other partial waves, one obtains three other ''physical'' states: an unbound p state near 0.2 MeV, a bound d state at -5.51 MeV, and a bound g state at -1.05 MeV. The simple potential (28) with a modified V_G simulates qualitatively a part of the bound ^{10}Be spectrum which displays a 2^+ state at -4.04 MeV and a 1^- state at -1.44 MeV. The fact that no bound state is obtained for the f wave beyond the forbidden state is not incompatible with a very weakly bound 3^- state at -0.04 MeV. The suggestion of the existence of a bound 4^+ state is more unexpected. We think that a reasonable approximation of the central part of the ^{6}He + α interaction can be obtained with a weak readjustment of V_G. A similar treatment of the α + α double-folding potential with the proper number of forbidden states provides a result very close to the accurate potential of Ref. [30]. However, in the ^{6}He + α case, the potential should involve an additional term depending on parity which we now discuss qualitatively.

Finally, we try to estimate the behavior of the parity-dependent potential component. This term is a direct consequence of Pauli antisymmetrization [31]. It can also be understood in an equivalent physical picture as arising from the elastic transfer of the halo neutrons [7]. Here, the Pauli principle applies to the identical α clusters. The order of magnitude of the decrease of this term is given by the overlap of two ^{6}He densities separated by a distance $2R/3$. Indeed, the parity term mostly arises from the overlap between an ^{6}He + α configuration and the same configuration inverted through the geometrical center of the system [31]. The factor 2/3 is exact in an harmonic-oscillator model but is only indicative here [32]. At large distances, the main effect should come from the overlap of the halo parts of the mirror ^{6}He wave functions. If these wave functions can be approximated at large distances by a product of individual orbitals for the external neutrons, this overlap is well approximated by an overlap between densities. Although the real halo wave function is much more complicated than this simple assumption, we qualitatively expect the asymptotic part of the parity term of the nucleus-nucleus potential to roughly decrease as

$$\int \rho(r)\rho(|\tfrac{2}{3}\mathbf{R}-\mathbf{r}|)d\mathbf{r} \underset{R\to\infty}{\propto} \exp(-\tfrac{2}{3}R/a), \qquad (29)$$

where $a \approx 0.7$ fm as obtained from Sec. III. Even with the uncertainties both on a and on the factor 2/3, one sees that the characteristic constant of this decrease should be larger than a and maybe as large as $3a/2$. The parity term should decrease more slowly, or at least not faster, than the tail of the potential (28) where a_S is equal to 0.725 fm. Therefore, the parity term might become dominant at some distance and have observable effects on the elastic cross section at large angles. However, the parity potential decreases with increasing orbital momenta [32] and its effects might be limited to a rather small energy domain near the Coulomb barrier. A more accurate study of the parity effect may require a microscopic wave function for the full ^{6}He + α system with antisymmetrization over the ten nucleons.

V. CONCLUSION

In preparation of the analysis of planned elastic-scattering experiments of a low-energy radioactive ^{6}He beam on an α target, we have determined a double-folding interaction between these nuclei with a realistic ^{6}He density derived from a microscopic calculation. This density might be useful, and is available, for calculations of interactions between ^{6}He and other nuclei.

The obtained ^{6}He + α potential displays an unusually long tail which should lead to observable effects on the cross sections. This real potential (with some possible renormalization for which we propose an estimate) should be useful as a real part of a phenomenological complex optical potential. A similar treatment of the neighboring α + α system provides an excellent approximation of realistic potentials and suggests that the present results should be useful. A reduction of the number of free parameters in the analysis of future elastic-scattering cross sections is essential in order to compensate for the limited angular range and accuracy of the first data. The complete optical potential is indeed expected to be rather complicated. Contrary to the α + α case, absorption should play an important role even at low energies because of the weak binding energy of ^{6}He. Moreover, a parity dependence of the potential due to the elastic transfer of the halo-neutron pair should also complicate the analysis.

The existence of a potential tuned on experimental data will allow one to make definite predictions on the existence of observable molecular resonances. Such resonances might indeed exist under the form of a loosely bound system made of a large ^{6}He cluster and an α particle. They should occur at larger mean distances than for the well-known 0^+ and 2^+ molecular resonances of ^{8}Be. These exotic objects should provide useful information on halo properties. If they exist, the optical potential should provide their locations and help in detecting them if they are too narrow to make observations easy. An important point here is the possible simultaneous existence of molecular resonances of both parities.

Performing a fully microscopic treatment of this collision with the resonating-group method (RGM) [8,9] is in principle possible but represents an important theoretical and numerical challenge. Tools for such a calculation can be developed within the existing techniques but the complexity of a realistic description of the ^{6}He wave function will make the calculation very heavy. The treatment of the open α + $\alpha + n + n$ channels should especially raise difficulties. Such a model calculation is nevertheless worth being attempted because the parameter-free RGM should provide accurate theoretical phase shifts and cross sections, if we can trust extrapolating the α + α case.

ACKNOWLEDGMENTS

This text presents research results of the Belgian program on interuniversity attraction poles initiated by the Belgian-state Federal Services for Scientific, Technical and Cultural Affairs.

[1] E. Liénard, D. Baye, T. Delbar, P. Descouvemont, P. Duhamel, W. Galster, M. Kurokawa, P. Leleux, I. Licot, P. Lipnik, C. Michotte, T. Motobayashi, A. Ninane, J. Vanhorenbeeck, and J. Vervier, Phys. Rev. C **52**, 775 (1995).
[2] I. Tanihata, H. Hamagaki, O. Hashimoto, Y. Shida, N. Yoshikawa, K. Sugimoto, O. Yamakawa, T. Kobayashi, and N. Takahashi, Phys. Rev. Lett. **55**, 2676 (1985); I. Tanihata, D. Hirata, T. Kobayashi, S. Shimoura, K. Sugimoto, and H. Toki, Phys. Lett. B **289**, 261 (1992).
[3] P.G. Hansen and B. Jonson, Europhys. Lett. **4**, 409 (1987).
[4] I. Tanihata, J. Phys. G **22**, 157 (1996).
[5] K. Riisager, Rev. Mod. Phys. **66**, 1105 (1994).
[6] M.J.G. Borge, L. Johannsen, B. Jonson, T. Nilsson, G. Nyman, K. Riisager, O. Tengblad, and K. Wilhelmsen Rolander, Nucl. Phys. **A560**, 664 (1993).
[7] W. von Oertzen and H.G. Bohlen, Phys. Rep. **19C**, 1 (1975).
[8] K. Wildermuth and Y.C. Tang, *A Unified Theory of the Nucleus* (Vieweg, Braunschweig, 1977).
[9] Y.C. Tang, in *Topics in Nuclear Physics II*, Lecture Notes in Physics (Springer, Berlin, 1981), Vol. 145, p. 572.
[10] A. Csótó, Phys. Rev. C **48**, 165 (1993).
[11] K. Varga, Y. Suzuki, and R.G. Lovas, Nucl. Phys. **A571**, 447 (1994).
[12] K. Varga, Y. Suzuki, and Y. Ohbayasi, Phys. Rev. C **50**, 189 (1994).
[13] Y.C. Tang, M. LeMere, and D.R. Thompson, Phys. Rep. **47C**, 167 (1978).
[14] M.V. Zhukov, B.V. Danilin, D.V. Fedorov, J.M. Bang, I.J. Thompson, and J.S. Vaagen, Phys. Rep. **231**, 151 (1993).
[15] D. Baye, M. Kruglanski, and M. Vincke, Nucl. Phys. **A573**, 431 (1994).
[16] D. Geddes, Travail de Fin d'Etudes, Université Libre de Bruxelles, 1992 (unpublished).
[17] P. Descouvemont, Phys. Rev. C **52**, 704 (1995).
[18] P. Descouvemont, Nucl. Phys. **A581**, 61 (1995).
[19] N.K. Timofeyuk, P. Descouvemont, and D. Baye, Nucl. Phys. **A600**, 1 (1996).
[20] D. Baye, Y. Suzuki, and P. Descouvemont, Prog. Theor. Phys. **91**, 271 (1994).
[21] Y. Suzuki, T. Kido, Y. Ogawa, K. Yabana, and D. Baye, Nucl. Phys. **A567**, 957 (1994).
[22] K. Varga and Y. Suzuki, Phys. Rev. C **52**, 2885 (1995).
[23] D. Brink, in *Many-Body Description of Nuclear Structure and Reactions*, Proceedings of the International School of Physics ''Enrico Fermi,'' Course 36, Varenna, 1965, edited by C. Bloch (Academic, New York, 1966), p. 247.
[24] D. Baye and P. Descouvemont, in *Proceedings of the Sapporo International Symposium on Developments of Nuclear Cluster Dynamics*, Sapporo, Japan, 1988, edited by Y. Akaishi *et al.* (World Scientific, Singapore, 1989), p. 6.
[25] D. Baye and P.-H. Heenen, J. Phys. A **19**, 2041 (1986).
[26] V.I. Kukulin and V.M. Krasnopol'sky, J. Phys. G **3**, 795 (1977).
[27] D.R. Thompson, M. LeMere, and Y.C. Tang, Nucl. Phys. **A286**, 53 (1977).
[28] D. Baye and N. Pecher, Bull. Cl. Sci. Acad. R. Belg. **67**, 835 (1981).
[29] D. Baye, P. Descouvemont, and N.K. Timofeyuk, Nucl. Phys. **A577**, 624 (1994).
[30] B. Buck, H. Friedrich, and C. Wheatley, Nucl. Phys. **A275**, 246 (1977).
[31] D. Baye, J. Deenen, and Y. Salmon, Nucl. Phys. **A289**, 511 (1977).
[32] D. Baye, Nucl. Phys. **A460**, 581 (1986).